CHAPTER VII

SYNTHESIS AND CHARACTERISATION OF CuI AND Mg-DOPED CuI NANOPARTICLES

7.1 Introduction

Electrochemical capacitors, also known as supercapacitor, (G. Wang et.al, 2012) are of great importance in electronic devices and power systems. Its high-power characteristics and long life cycle makes them desirable as energy storage and delivery device. Unlike conventional capacitors where the capacitance depends solely on the solid dielectric, the capacitance value of an electrochemical capacitor is determined by two storage principles: electric double layer capacitance (EDLC) and pseudocapacitance, both of which contribute to the total capacitance of capacitor (N. Devillers et.al 2014, Y. Zhang et.al 2009, A. Burke 2000). CuI have found various applications in solar cells and catalysis, but the studies on electrochemical capacitive properties of CuI is limited.

In this work, the electrochemical impedance analysis of magnesium doped CuI NPs is studied using impedance spectroscopy (EIS). The electrochemical studies reveal that the CuI-Mg electrode is a potential material for supercapacitor application in addition to its other numerous applications.

7.2 Experimental Methods

7.2.1 Materials

All the chemicals used in our experiments were of analytical grade and were used without any further purification. Copper (II) chloride dihydrate ($CuCl_2.2H_2O$) procured from Merck, potassium iodide and Sodium thiosulfate from Himedia were used in our experiments. Magnesium (II) chloride hexahydrate was purchased from Merck. Deionized water was used throughout the experiment.

7.2.2 Characterization

The X-ray diffractions (XRD) of undoped and Mg-doped CuI films were obtained on PANalytical X'Pert PRO powder X-ray Diffractometer, at a scanning range of 20-80°with CuKα radiation of wavelength λ =1.5406 Å. The UV-DRS spectra of the films were obtained at room temperature using Agilent CARY 500 UV-VIS-NIR spectrophotometer in the wavelength range of 300-1100 nm. The room temperature photoluminescence spectra of the films were recorded on SHIMADZU RF-6000 spectrofluorophotometer in the range of 400-800 nm at the excitation wavelength of 325 nm. Electrochemical impedance analysis of the nanoparticles was performed using CHI660C electrochemical workstation over frequency range of 0.1 Hz – 0.1 kHz by applying an ac signal of 5 mV in amplitude throughout the experiment. A three-electrode configuration was employed in the measurement where nanoparticles coated ITO-glass electrode served as the working electrode, saturated Ag/AgCl as the reference electrode and platinum foil as the counter electrode.

7.2.3 Synthesis of CuI and Mg doped nanoparticles

In a typical synthesis, 100 mL of 0.5 M reducing agent sodium thiosulphate solution was added in drops to 100 mL of 0.5 M aqueous solution of copper (II) chloride dihydrate solution with constant stirring. To the stirred solution, aqueous solution of potassium iodide is added drop by drop and a brown colour precipitate is formed, which was filtered, washed and dried in oven at 60^{o}C for 4 hours.

The Mg doped CuI nanoparticles was prepared by conventional precipitation method. About 50 mL of 0.5 M reducing agent sodium thiosulphate solution was added in drops to the solutions containing 50 mL of 0.5 M aqueous solution of copper (II) chloride dihydrate solution and 5 mol% and 10 mol% aqueous solution of magnesium (II) chloride hexahydratewith constant stirring. To the stirred solution, aqueous solution of potassium iodide is added drop by drop and a brown colour precipitate is formed, which was filtered, washed and dried in oven at 60^{o}C for 4 hours.

7.3 Results and discussion

7.3.1 X-ray diffraction studies

Figure 7.1 shows the powder XRD patterns obtained for CuI and Mg-doped CuI nanoparticles. The peaks observed in the XRD pattern of pure and Mg-doped CuI nanoparticles are in good agreement with the reported standards (JCPDS card no. 76-0207). The characteristic peaks at 2θ values 25^{o}, 29^{o}, 42^{o}, 50^{o}, 61^{o}, 67^{o}, 69^{o} and 77^{o} could be indexed to the (111), (200), (220), (311), (222), (400), (331) and (420) planes of γ-CuI and Mg-doped NPs which is in accordance with that of the γ phase of copper iodide in zinc blende crystal structure. The doped nanoparticles are found to be phase pure however with significant change in crystallinity as

observed from significant reduction in the peak intensities. The particle size D of the samples was determined using the Scherrer formula

$$D = k \lambda / \beta \cos \theta$$

where d, λ, θ, and β denote the mean crystallite size, the X-ray wavelength (1.5406 Å) incident angle and full width at half maximum (FWHM) respectively. The calculated crystallite size of the undoped and 5 mol% and 10 mol% doped CuI nanoparticles are found to be 46, 42 and 30 nm respectively. The crystallite size decreases with increasing dopant concentration.

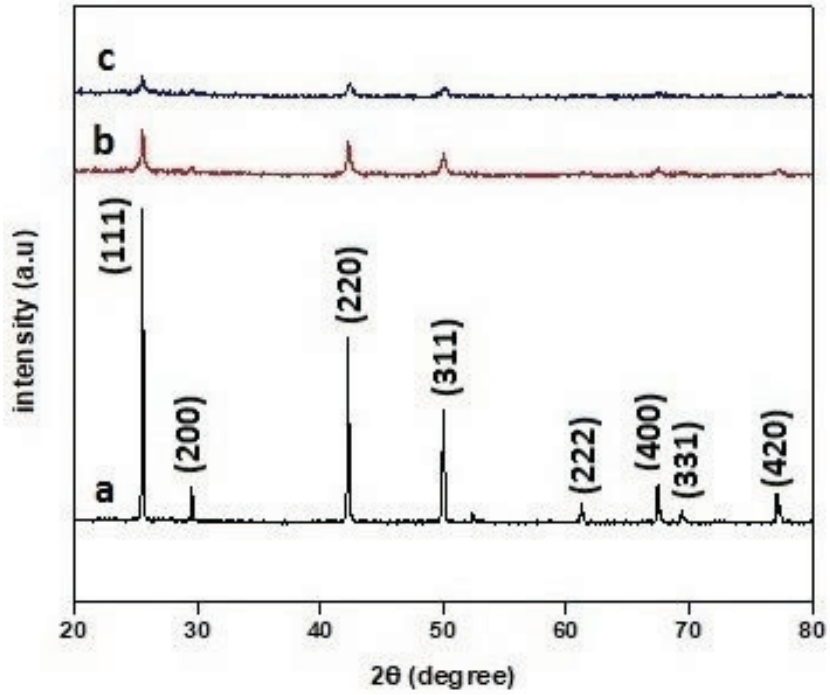

Fig 7.1 X-ray diffractograms of (a) CuI (b) 5 mol% Mg-doped CuI (c) 10 mol% Mg-doped CuI nanoparticles.

7.3.2 UV-DRS studies

Fig.7.2 portrays the absorption spectra of the as-prepared CuI and Mg doped CuI samples. Doping of Mg shifts the absorption onset to near UV region (400-350 nm) extending the optical window. Moreover, with the increase in Mg concentration, the band edge shifts to the side of higher energy (C. H. Ku et.al 2005, Y. S. Wang et.al 2006). The systematic shift with doping levels suggests that the introduction of dopant ions with marginal contribution from size effects bring about these changes (Y. F. Yang et.al 2010, B. Karthikeyan 2010). We therefore attribute the origin of the increase in transmittance to the influence of dopant ions. Moreover, with the increase in concentration of Mg, the bands get shifted towards the shorter wavelength (higher energy).

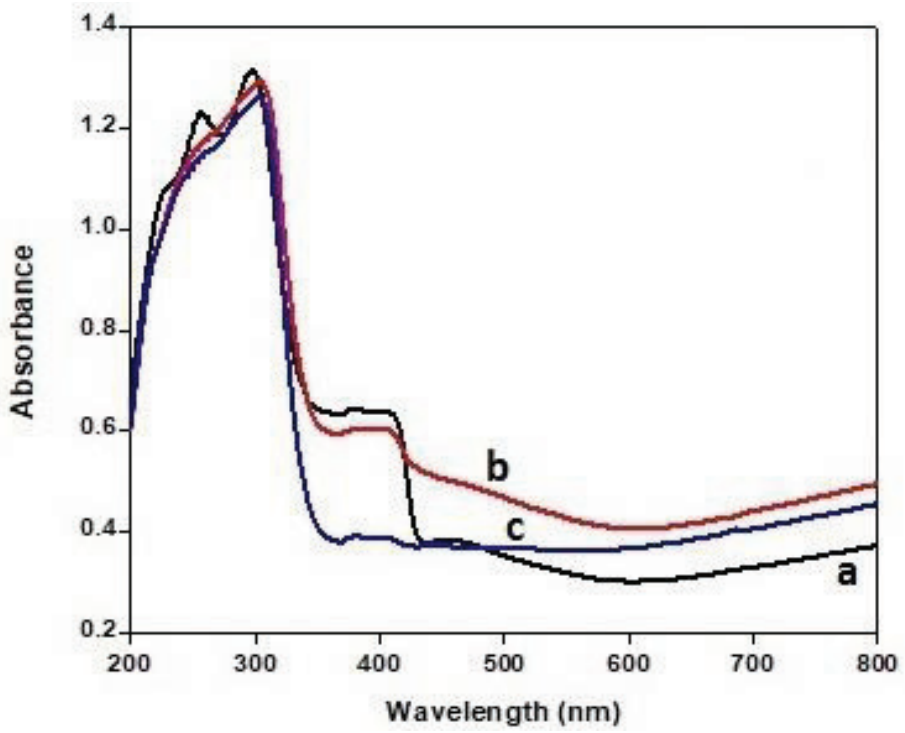

Fig 7.2 Absorbance spectra of (a) CuI (b) 5 mol% Mg-doped CuI (c) 10 mol% Mg-doped CuI nanoparticles

Optical bandgap energies of the prepared samples were obtained from Tauc relation given by

$$\alpha h\nu = A'\left(h\nu - E_g\right)^n$$

where α =2.303A/t is called the coefficient of absorption, A being the absorbance and t, the optical path length, A′ is called proportionality constant, E_g being the bandgap energy, hν is the energy of photon and for direct transition the value of n is found to be 1/2. From the Tauc plots (Fig. 7.3), it can be observed that the bandgap of undoped CuI films is 3.1 eV and that of 5 mol% and 10 mol% Mg doped CuI nanoparticles are and 3.9 and 4.08 eV respectively.

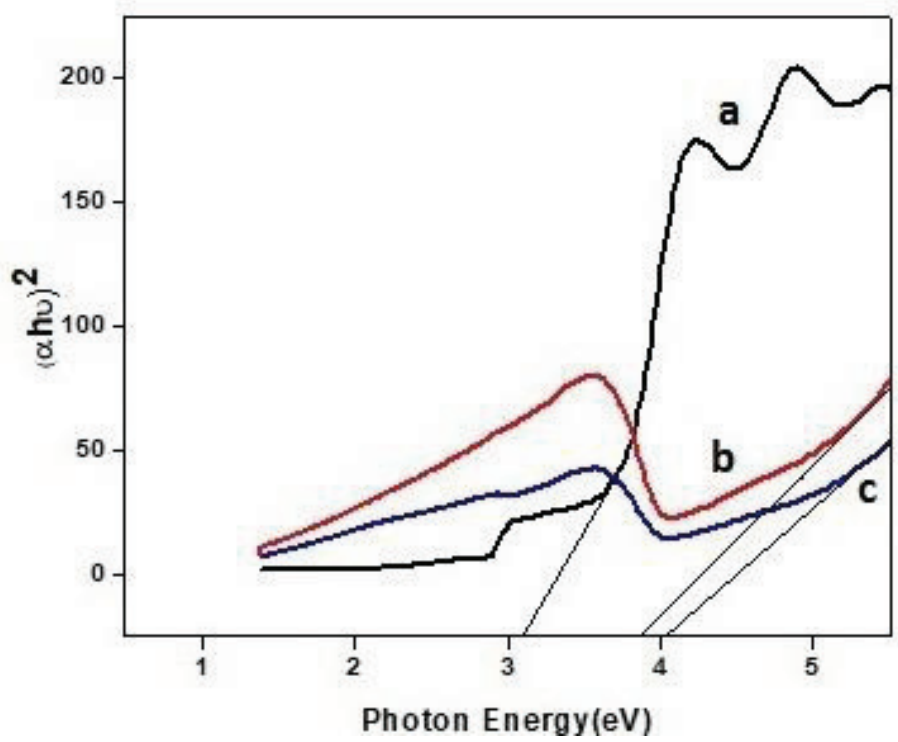

Fig 7.3 Tauc plots showing the variation of $(\alpha h\nu)^2$ with photon energy for (a) CuI (b) 5 mol% Mg-doped CuI (c) 10 mol% Mg-doped CuI nanoparticles.

7.3.3 Electrochemical impedance Analysis

The plot of frequency against the phase angle is shown in the Bode plot (Fig 4,5,6). The CuI electrode shows a maximum phase angle of 26° and for doping of 5 mol% concentration of Mg, the phase angle rises to 42° which on further doping the phase angle decreases to 36°. These values confirm the pseudocapacitive nature of the electrodes. Doping introduces slight difference in the phase angles of the CuI nanoparticles.

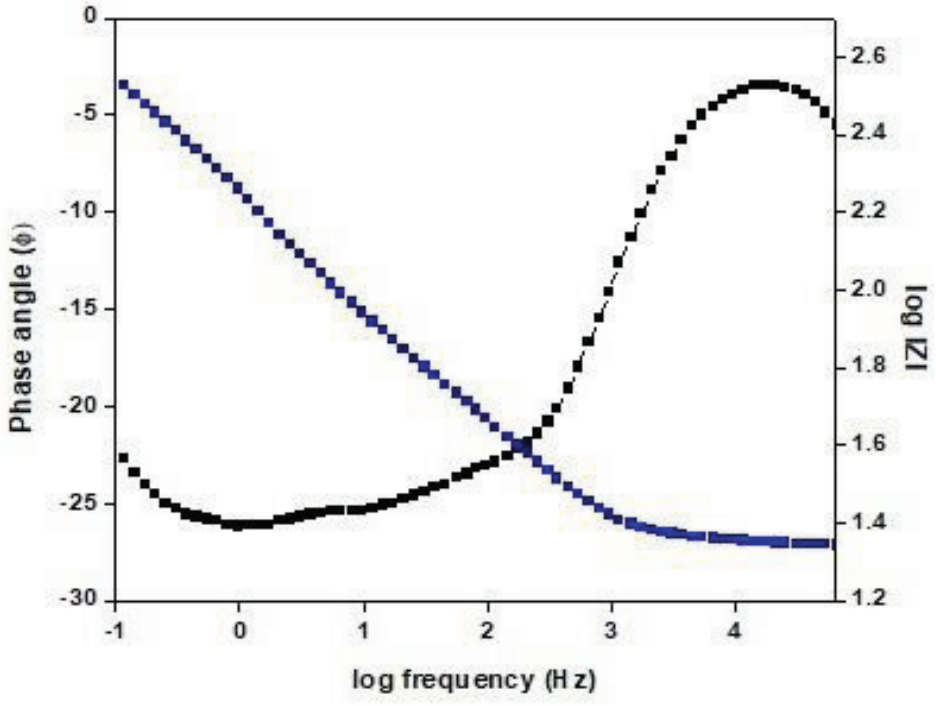

Fig 7.4 Bode plot of CuI nanoparticles

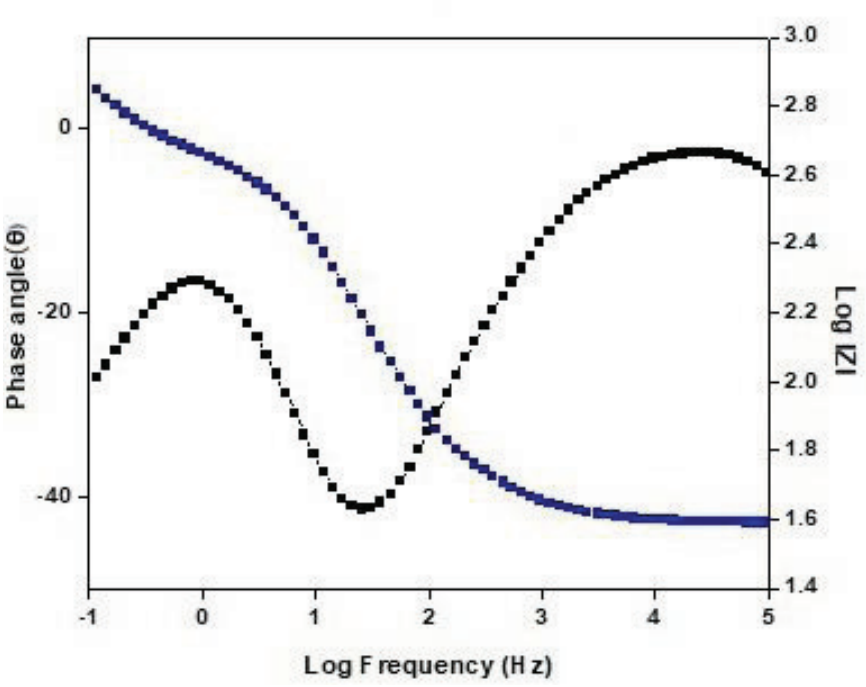

Fig 7.5 Bode plot of 5 mol% Mg doped CuI nanoparticles

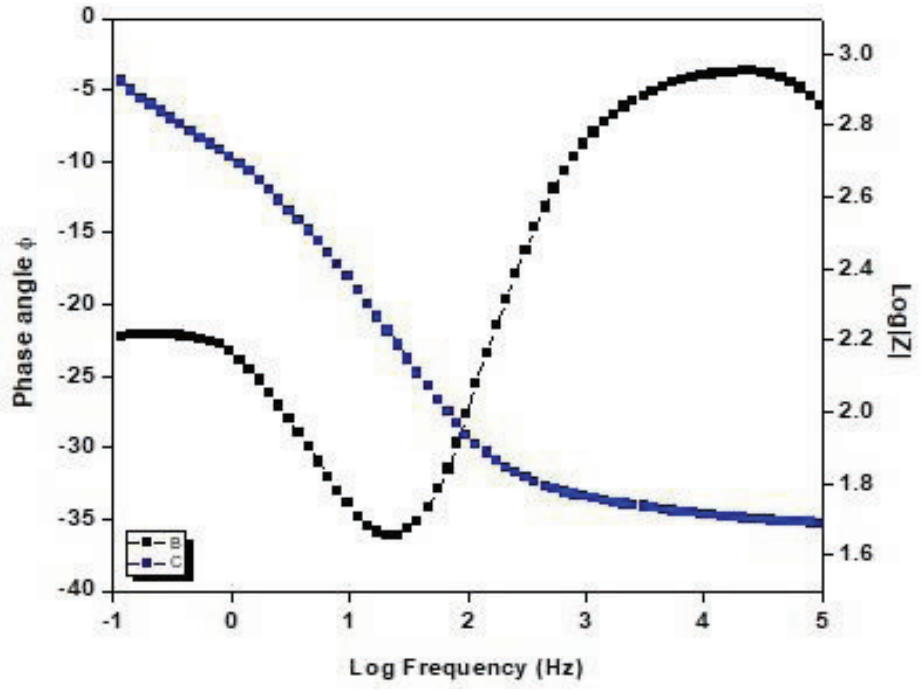

Fig 7.6 Bode plot of 10 mol% Mg doped CuI nanoparticles

The magnitude of impedance (|Z|) decreases in all the samples with respect to increase in frequency due to the frequency dependence of capacitive reactance. At low frequencies, the Warbug impedance characteristic is observed in the samples due to the significant charge transfer resistance and diffusion related process. From the observed characteristics, the circuit for pure CuI is equivalent to R_1C component in series where R_1 is the equivalent series resistance (ESR) and C is the double layer capacitance. In case of doped samples, the equivalent circuit is observed to be a parallel R_2C component in series with a resistance R_1 along with Warburg impedance, where R_1 is the equivalent series resistance (ESR) and R_2 is the charge transfer resistance. In the low and mid frequencies, the capacitive behaviour is dominant while it gives purely resistive at high frequencies.

In phase angle *vs* log frequency plot, the phase angle reaches a maximum for a particular frequency showing a dominant capacitive behaviour and then the resistive component becomes more pronounced on increasing the frequency finally turns purely resistive at higher frequencies. From the Bode's plot, the maximum phase angle is observed in 5 mol% Mg-doped samples and hence dominant capacitive behaviour is perceived in this sample.

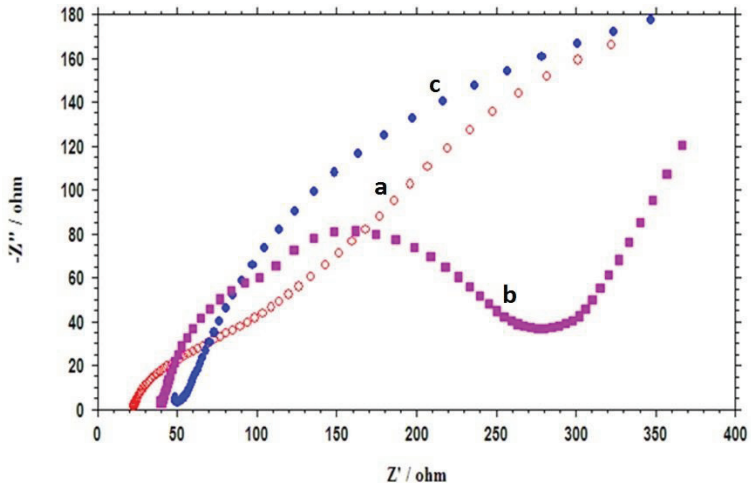

Fig 7.7 Nyquist of (a) CuI (b) 5 mol% Mg-doped CuI (c) 10 mol% Mg-doped CuI nanoparticles

The Nyquist plot obtained at a frequency range of 0.1 Hz to 0.1 MHz at constant voltage amplitude of 5 mV is shown in fig 7.7. The impedance analysis of the samples is an indicative of the combination of kinetic and diffusion controlled processes in the electrochemical characteristics. The equivalent circuit of the observed impedance characteristics is shown in Fig 7.8.

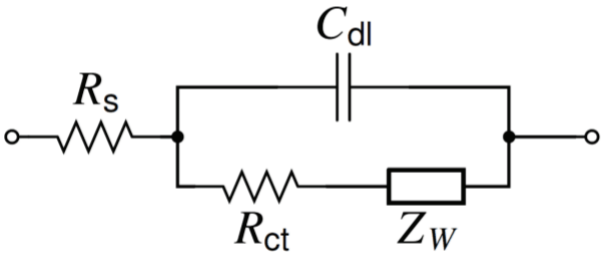

Fig 7.8 The equivalent circuit showing solution resistance (R_s), double layer capacitance (C_{dl}), charge transfer resistance (R_{ct}), and Warbug impedance (Z_w)

The bulk resistance (ESR) can be determined from the intercept on the real axis (Z') in the high frequency region, which is 20Ω, 40Ω and 50Ω for the undoped, 5 mol% and 10 mol% doped CuI samples respectively. The difference in the ESR values is due to the difference in the conductance of electrode materials. For 5 mol% Mg doped CuI, the radius of semicircle, as observed from the Niquist plot, is considerably reduced leading to significant charge transfer resistance compared to other samples. Though 10 mol% Mg doped sample shows lesser capacitive behaviour, it shows significant improvement over pure CuI sample (R. Suresh et.al 2016, Afshin Pendashteh et.al 2013).

The contribution of warbug impedance at lower frequency region indicating mass transfer control is seen in both undoped and doped samples. The domination of Warburg impedance in 5 mol% doped CuI could be due to the higher charge transfer resistance compared to 10 mol% doped sample (A. J. Bard et.al 2001, Su-Moon Park et.al 2003, M. E. Orazem et.al 2008).

7.4 Conclusion

In summary, pure CuI nanoparticles and magnesium doped nanoparticles have been prepared by conventional precipitation method. The prepared undoped and doped nanoparticles are characterized to compare the change in optical and electrochemical properties on doping. The powder XRD patterns confirm the formation of the phase purity of the samples and the crystallite sizes are 46, 54 and 30 nm for undoped and doped samples. In UV-visible absorption spectra, the absorption edge for Mg-doped films is blue shifted compared to undoped CuI films increasing the transmission window. The Bode plot of 5 mol% doped sample showed maximum phase angle of 40^{o}at a lower frequency showing better electrochemical properties compared to other samples. From the electrochemical impedance studies, it is observed that the equivalent series resistance (ESR) increases (20Ω, 40Ω and 50Ω) with doping. In particular, impedance increases initially with 5 mol% of Mg which on further doping takes a value in between pure CuI and 5 mol% doped sample. Hence the increase in dopant concentration improves the capacitive behaviour of Mg doped CuI nanoparticles.